CSO MS-39: Principles and Applications

29

Gabriele Vestri, Francesco Versaci, and Giacomo Savini

Introduction

Tomographers based on Scheimpflug technology had the undoubted merit of extending the diagnostic capabilities of Placido corneal topographers, which were limited to an accurate automated measurement in one single shot of a large area of the anterior corneal surface. Indeed, they enabled the imaging of whole anterior segment sections, thus adding visual and quantitative information on the posterior corneal surface and on the anterior chamber (iris, angles, and anterior part of the crystalline lens). With these advancements, clinicians were able to get new information about their patients: elevation maps of the anterior and posterior corneal surfaces and pachymetric maps to detect keratoconus and ectasia, posterior and total corneal astigmatism to plan toric intraocular lenses (IOLs) implantation, calculation of total corneal power by ray tracing to compute IOL power after corneal refractive surgery. Nevertheless, the main limitations of Scheimpflug technology were the low resolution, the poor quality of anterior segment scans, and the presence of artefacts due to an excessive amount of tissue scattering. MS-39 was conceived to overcome the previous limitations thus allowing for the acquisition of high-quality angle-to-angle images of the anterior segment. The superior quality of the images, in particular the improved detail of corneal layers, offers the clinician new opportunities for early keratoconus detection, preoperative and postoperative management of corneal transplantations, refractive surgery, and orthokeratology.

Technical Features of MS-39

MS-39 is a topographer-tomographer (Fig. 29.1), which puts together a Placido disc [1] and a FD-OCT (Fourier domain optical coherence tomography) system [2–4]. Placido disc is solely

Fig. 29.1 CSO srl, MS-39

G. Vestri (✉) · F. Versaci
CSO s.r.l., Florence, Italy
e-mail: g.vestri@csoitalia.it; f.versaci@csoitalia.it

G. Savini
IRCCS Bietti Foundation, Rome, Italy

Studio Oculistico d'Azeglio, Bologna, Italy
e-mail: giacomo.savini@startmail.com

J. Aramberri et al. (eds.), *Intraocular Lens Calculations*, Essentials in Ophthalmology,
https://doi.org/10.1007/978-3-031-50666-6_29

used for the topography of the anterior corneal surface, while the OCT system is used for the topography and tomography of the anterior ocular segment. The Placido technology is based on the principle of reflection of a known pattern of rings on a curved mirror, which is the anterior corneal surface. A proper processing of their reflected image on the corneal surface allows for an accurate measurement of its shape.

The OCT system is specifically a SD-OCT (spectral domain), which is based on the interference of two beams of a broadband infrared radiation coming from a reference arm and a sample arm. The basic scheme of a SD-OCT (Fig. 29.2) system is made up of a broadband radiation source, an interferometer with four arms, a spectrometer for collecting the interference signal, a processing unit that transforms the interference signal into a tomographic image. One arm of the interferometer is the entry of the broadband radiation. A second arm (reference arm) is used for creating a reference in distance and for generating one of the interfering beams. The third arm (sample arm) is for launching the radiation toward the sample and for collecting its backscattered beam. The fourth one (detection arm) is for collecting the interference of the beams coming from the reference and sample arms into a spectrometer.

In MS-39, the broadband source is an infrared superluminescent diode (SLD) emitting a radiation centered around 850 nm. This is splitted by the interferometer toward the reference and sample arms. At the end of the reference arm, a fixed mirror reflects the beam back toward the detection arm where the spectrometer collects it. Similarly, the radiation transmitted to the sample arm is pointed toward a certain direction outside the instrument by an X–Y scanning system and, then, backscattered by the ocular tissues toward the detection arm, where it interferes with the beam back-reflected by the reference arm. For each wavelength available in the source, the sensor of the spectrometer collects the intensity of a beam generated by the constructive, destructive, or partially constructive interference of the two

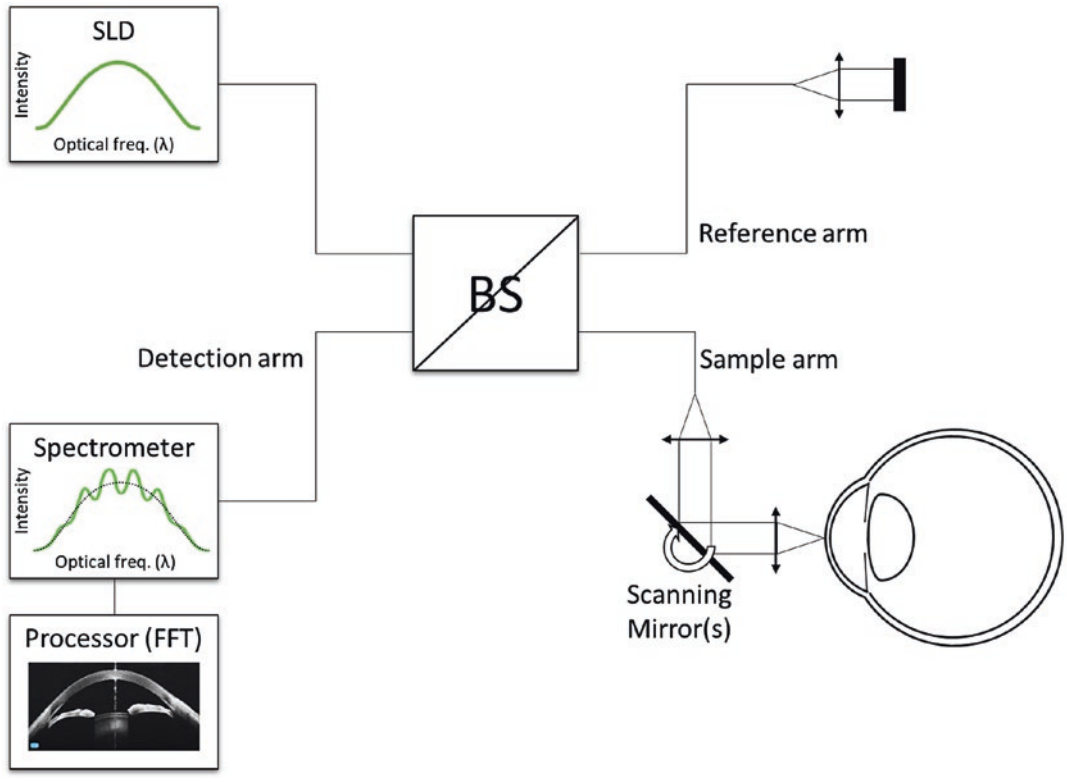

Fig. 29.2 Basic scheme of SD-OCT

beams coming from the reference and sample arms. The set of these values at various wavelengths is processed with a proprietary algorithm, basically containing a Fourier transformation, to obtain the reflectivity profile of the sample along the axis of the scanning beam. Therefore, in a single shot, the sensor of the spectrometer collects the spectrum necessary to determine the profile of reflectivity along one axis of the sample. The spectrometer inside the instrument collects an interval of wavelengths of about 80 nm thus ensuring an axial pixel size of 4.8 μm in air (about 3.5 μm in tissue) and an imaging depth of about 10 mm in air. The scanning system is based on two galvanometric mirrors, which deviate the beam according to the numerous preset trajectories, and allows a maximum transversal field of 16 mm and a transversal resolution of 35 μm.

SD-OCT technology was chosen for the MS-39 instead of the SS-OCT (Swept Source), even though the latter has already shown some undeniable advantages like a higher scan rate and a greater imaging depth because it allows for an axial resolution that is less than half that of the best SS-OCT systems (5 μm instead of 13 μm, respectively). High-resolution Scheimpflug cameras can hardly provide an axial resolution at least double than the one of SS-OCT instruments. To the best of our knowledge, the axial pixel size of the MS-39 is currently the highest of all the OCT instruments available on the market, be they designed for the anterior segment or retina. It has to be emphasized that this feature is extremely important to resolve details in corneal layers, in particular for the epithelium. The imaging depth of the MS-39 is also the highest of all the ophthalmic SD-OCT instruments on the market.

Even though the axial resolution of the OCT system is high, it was necessary to integrate it with a Placido disc to get a reliable measurement of the height and curvature of the anterior corneal surface. To explain better this choice, let us consider the height profile of two spheres with curvatures of 42.50 D and 42.75 D (7.94 and 7.89 mm), i.e., differing by 0.25 D in curvature. The height difference between two meridional sections of the two spheres is about 0.06 μm at 0.4 mm from the center, 0.6 μm at 1 mm, 1.6 μm at 2 mm (Fig. 29.3). If these values are compared with the axial pixel size of the OCT system in air and if

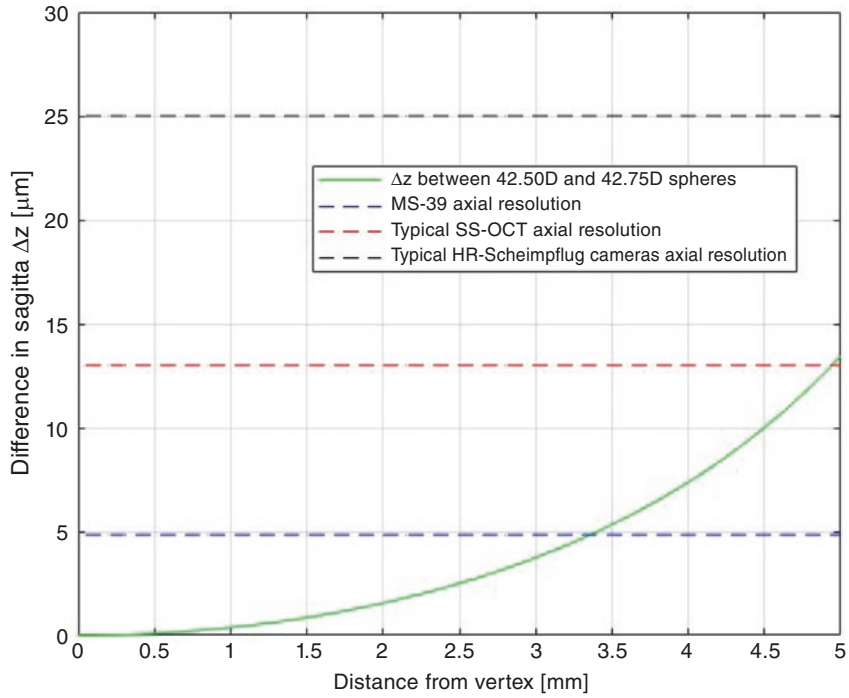

Fig. 29.3 Difference in the height profile of two spheres with curvatures of 42.50 D and 42.75 D (7.94 μm and 7.89 μm)

we consider that one of the primary purposes of the instrument is the accurate measurement of corneal surfaces, the need to add a Placido disc immediately becomes clear. In MS-39 software, for all cases where the keratoscopy is available and reliable (i.e., the anterior corneal surface is not very irregular or damaged), the measurement of the anterior surface obtained with Placido disc is preferred to the measurement done with the OCT system.

As regards the wavelength choice, MS-39 adopts a radiation source centered around 850 nm instead of the longer wavelength 1310 nm used in anterior segment OCT devices of other competitors. It was preferred to improve the image detail in corneal layers rather than the penetration into tissues, which would have had the advantage of imaging deeper structures such as the scleral spur or the posterior surface of the iris. At 850 nm the corneal epithelial layer is perfectly delineated, as it is the case for the transition from cornea to conjunctiva in the limbal region. Details of the normal structure of the stroma, including minimal changes of transparency approaching the limbal area, can be fully appreciated thanks to the 850 nm wavelength of the instrument, close to that of visible light. The iridocorneal angle and the iris stroma down to the posterior pigmented epithelium, as well as the crystalline lens within the pupillary aperture, can be visualized in fine detail. Unfortunately, no OCT can penetrate the eye beyond the iris pigmented epithelium, even those utilizing longer wavelengths, leaving the investigation of other ocular structure (e.g., ciliary body tumors) to other more invasive means, including ultrasounds, CT, and MRI.

Acquisition

MS-39 offers a wide range of different acquisition modalities, which allow the clinician to fully exploit the diagnostic potential of the instrument.

Section

This important modality recalls the use of the slit lamp, but with the fundamental difference that the captured images, based on OCT scanning technology, can be suitable for accurate measurements.

Two options are available for choosing the image quality:

- High definition: several images of the same section are captured in order to calculate an average image where the presence of the speckle is drastically reduced.
- Raw image: this option is faster than the previous one as there is no averaging of multiple pictures; it is useful when the patient is not very cooperative in order to reduce the acquisition time.

The sectional images can be acquired at various orientations (Fig. 29.4a) by selecting the angle through a rotating wheel on the top of the joystick or by clicking the desired direction on the enface corneal image shown on the screen.

The width of the transversal field of view can be chosen by the user between two options 10 and 16 mm, respectively, dedicated to the analysis of details in the layers of a limited corneal portion and to the overall view of the anterior segment.

In order to influence the pupil dilation, three illuminating conditions of the eye are available during the acquisition: scotopic, mesopic, and photopic.

In order to speed up the daily workflow of a clinical practice, some preset scanning patterns are made available:

- 2×: two sections at 90° degrees are acquired, one in the horizontal and one in the vertical direction (Fig. 29.4b).
- 4×: four sections are acquired at equispaced angular orientations, one at 0°, one at 45°, one at 90°, and one at 135°(Fig. 29.4c).

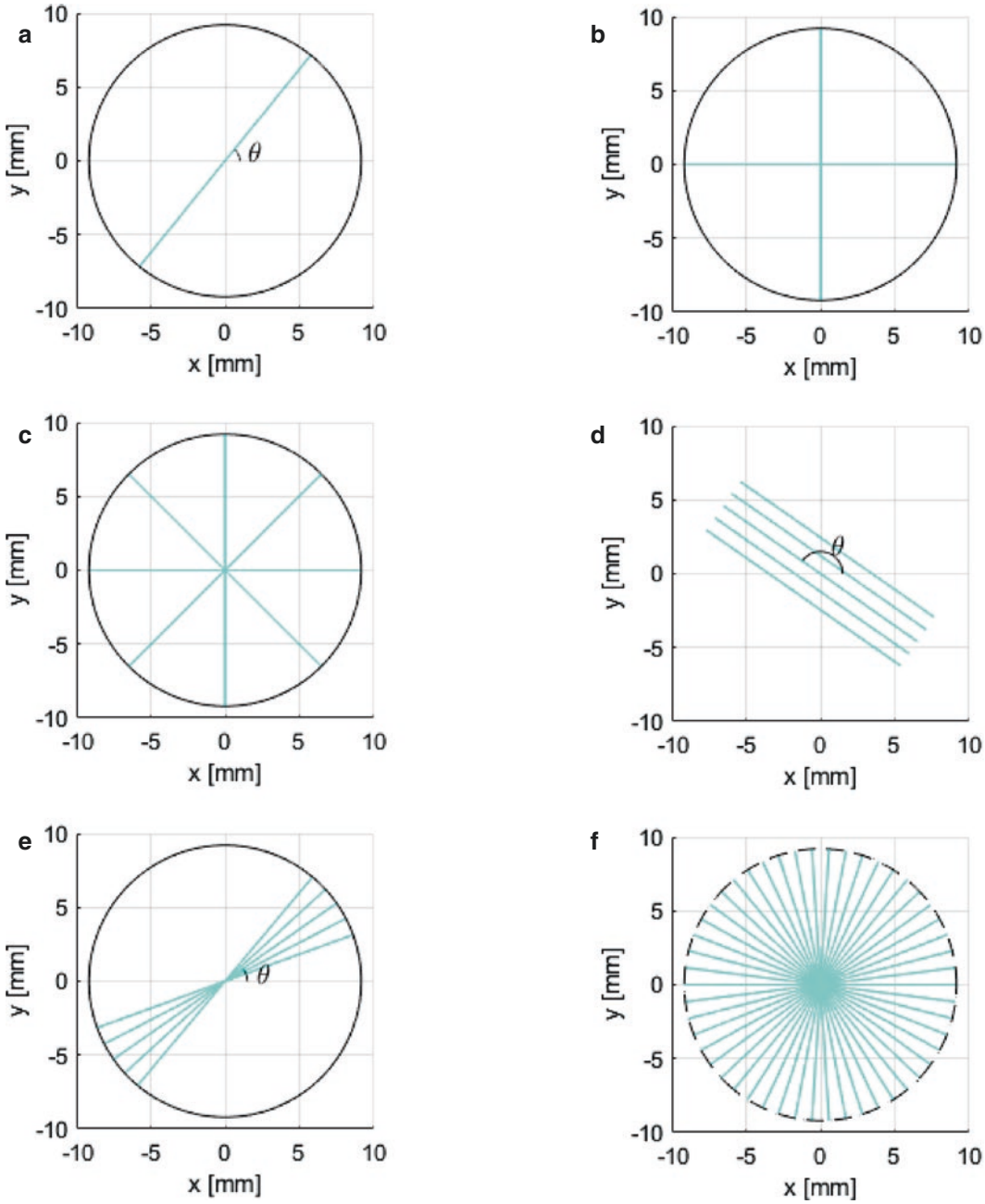

Fig. 29.4 *Scanning patterns*: (**a**) Line scanning, (**b**) horizontal and vertical lines (2×), (**c**) four meridians (4×), (**d**) raster scanning with 5 lines and interdistance equal to 1 mm, (**e**) sector scanning with 5 lines, (**f**) star scanning for topography (25 sections)

- Raster: an odd number of sections (from 3 to 7) are captured at an orientation and interline distance chosen by the user. The interline distance can be adjusted from 0.3 to 1 mm (Fig. 29.4d).
- Sector: an odd number of images (from 3 to 7) can be captured at equispaced angles within a sector, whose orientation and angular amplitude can be chosen by the user (Fig. 29.4e).

In cataract surgery, this exam may be important for detecting possible conditions which would be not clearly visible with other instruments like slit lamps or Scheimpflug tomographers, e.g., endothelial detachments, secondary cataracts, corneal oedemas, and capsular bag distension syndromes. Some interesting examples are reported in Figs. 29.5, 29.6 and 29.7.

Last but not least, a section video modality is made available for capturing nonstationary phenomena. It can be helpful, for instance, in analyzing the iris motion and the possible closure of the irido-corneal angle (dynamic gonioscopy), the ICL vaulting changes at standardized luminous conditions or to document the presence of floating elements in the aqueous (e.g., fibrins after cataract surgery), as shown in Fig. 29.8.

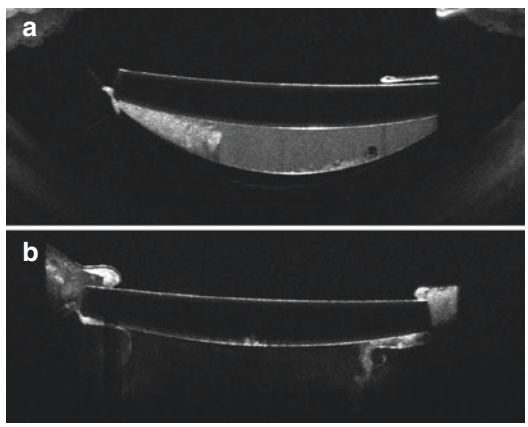

Fig. 29.5 (**a**) the AS-OCT shows the hyperscattering material between the IOL and the posterior capsule, which is distended towards the vitreous. This image helps the clinician to differentiate the capsular bag distension syndrome from a more common posterior capsule opacification. (**b**) After Nd:Yag laser capsulotomy, the milky liquid immediately disappeared. The patient's refraction changed from −0.75 D to plano and uncorrected visual acuity changed from 20/50 to 20/20

Lens Biometry

This acquisition mode is for the analysis of the crystalline lens. In this case, two sections, one horizontal and the other vertical, are acquired over a width of 16 mm. This exam is used to check the lens transparency, detect possible cataracts, and for measuring the lens thickness and estimating the position of its equatorial plane. These measurements can be useful as input data for those IOL calculation formulas, which require the knowledge of the crystalline lens for the prediction of the IOL position.

Pupillography

MS-39 offers a specific examination for the measurement of pupil position and diameter in several light conditions: scotopic, mesopic, photopic, and dynamic (i.e., during the transition from a high-photopic to a scotopic condition). This exam, often underestimated or completely neglected in the clinical practice, is very important for the assessment of the optical quality of the anterior ocular segment particularly in com-

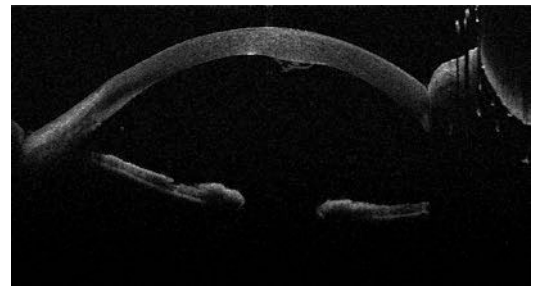

Fig. 29.6 A post-traumatic flap of the corneal endothelium is clearly imaged by the AS-OCT scan. Serial follow-up enabled the clinician to see the progressive recovery of the endothelium, which was fully adherent to the stroma after air injection into the anterior chamber

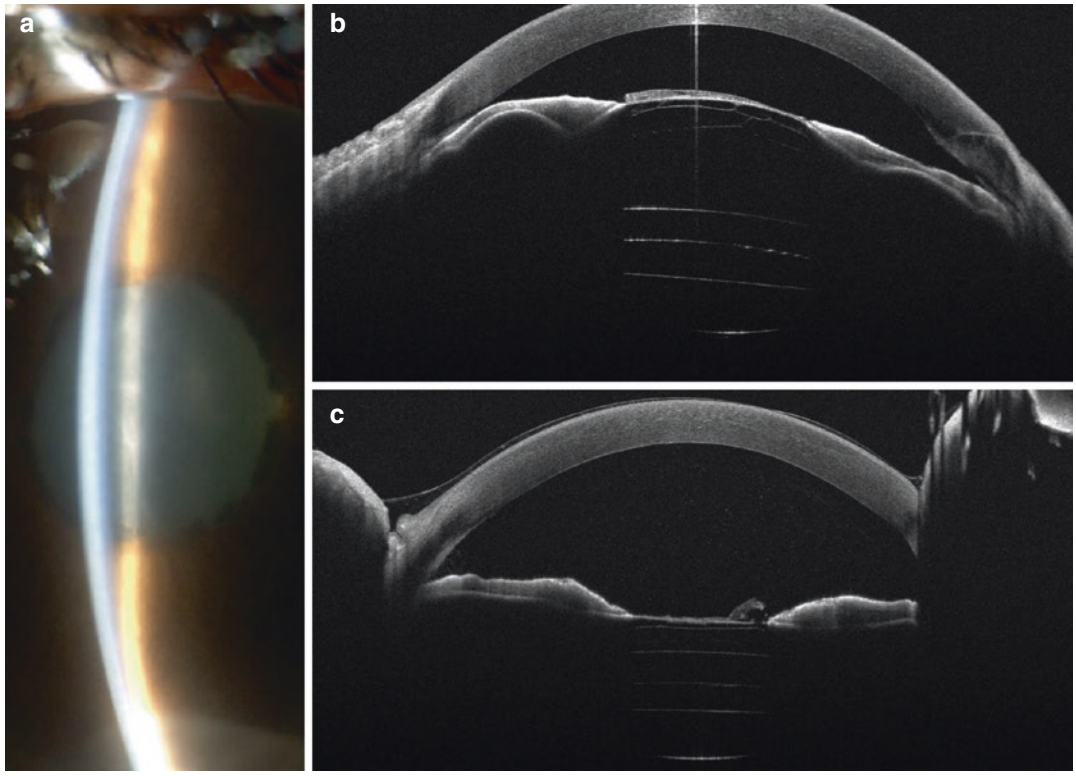

Fig. 29.7 (**a**, **b**) Pupillary block due to fibrin subsequent to TASS in a patient that received an add-on IOL in the sulcus. (**c**): Immediately after YAG laser application on the fibrin membrane, the block resolved and the anterior chamber depth returned physiological. The hole caused by the laser can be observed on the right of the scan

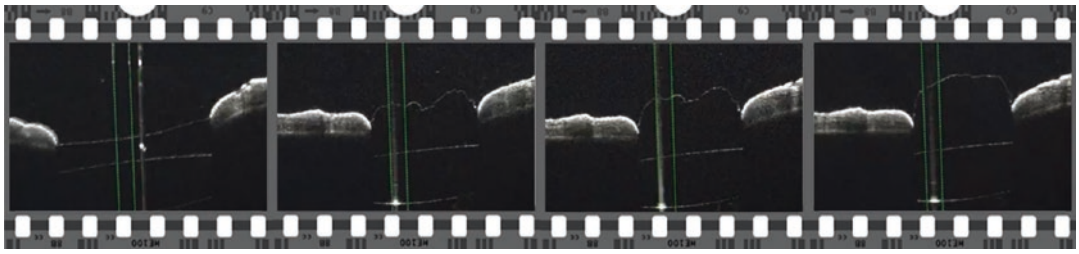

Fig. 29.8 A thin fibrin membrane occluding the whole pupillary area the first day following cataract surgery can be visualized, and its movements observed while protruding in the anterior chamber when pupillary constriction is elicited by light

bination with a corneal topography. Specific applications can be the pre-operative evaluation of a candidate for refractive surgery or the decision on whether to implant a multifocal or an aspheric IOL or the postoperative evaluation of the optical zone after refractive surgery.

Topography

The topography acquisition modality is for collecting the images necessary for the measurement of the anterior ocular segment, i.e., for the calculation of the classical curvature, power, and

height maps of the corneal surfaces and of the anterior chamber depth.

Three options are available for the OCT star scanning pattern of meridional sections at equally spaced angular positions:

1. 25 B-scans, each made up of 1024 A-scans, of 16 mm sections captured in a time lapse of about 1 s (Fig. 29.4f).
2. 12 B-scans over a width of 16 mm, each made up of 1024 A-scans and resulting from the average of the 2 images of the same meridian, captured in a time lapse of about 1 s.
3. 12 B-scans over a width of 10 mm, each made up of 600 A-scans and resulting from the average of 5 images of the same meridian, captured in a time lapse of about 1.5 s.

The second and third options can be used to produce higher-quality images over the full transverse field or a reduced central portion of it.

During the OCT scan, two frontal images of the eye, one for keratoscopy and the other of the iris, are also captured with a field of view of about 14.1 × 10.6 mm.

As an evolution of the CSO Sirius topographer-tomographer, the MS-39 is able to measure all the classical maps of the anterior ocular segment (Fig. 29.6):

- Axial and tangential curvature maps of both anterior and posterior corneal surfaces
- Altimetric difference maps of both anterior and posterior corneal surfaces respect to a reference spherical, conicoidal, or toric surface
- Refractive power maps for both corneal surfaces alone and for the whole cornea
- Corneal thickness
- Anterior chamber depth
- Gaussian curvature maps for the anterior and posterior corneal surfaces
- Wave front error maps for the whole cornea and its components due to the anterior and posterior corneal surfaces

Accurate topographic maps may be useful in cataract surgery planning in order to discriminate between a normal case, where third- and fourth-generation IOL formulas are sufficiently reliable, and a complex case, where it is necessary to adopt an eye model more refined than simple keratometries and a ray tracing calculation for the choice of the best IOL. Topographic maps are also necessary for planning a refractive retreatment, when the optical quality of cornea should be improved before cataract surgery in order to have a satisfactory visual quality after the IOL implant. This is, for example, the case of eyes with a decentered optical zone due to an imperfect former refractive surgery or in some cases of corneal irregularity due, for instance, to corneal grafts.

In MS-39 software topographic maps are accompanied by a great number of synthetic indices. Some of them refer to corneal morphology (keratometries and shape indices), some other to corneal optical quality (refractive indices), and some other to generic features of the anterior segment. Among them, the software offers the measurement of the horizontal tilt component of the iris plane. This can be useful in cataract surgery for the prediction of the tilt of the implanted IOL. Tilt of intraocular lenses has a negative effect on optical performance, especially for aspheric, toric, and multifocal IOLs and lead to less predictable astigmatism outcomes after surgery. An improved ability to predict postoperative tilt would help determine the best IOL for a patient and potentially improve long-term outcomes.

By exploiting its superior imaging capability in resolving corneal layers, the MS-39 is also able to calculate the epithelial and stromal thickness maps over a diameter of 8 mm (Fig. 29.9). It is by now widely acknowledged that epithelial thickness maps can be used as an adjunctive tool to improve the sensitivity and specificity of keratoconus screening [5–10].

During preoperative assessment for refractive surgery, epithelial thickness mapping can be very valuable at least in two situations. First, it can correctly detect or confirm a keratoconus diagnosis for those patients where their anterior surface topography may be clinically judged within normal limits and their posterior surface topography is outside normal limits. Epithelial information

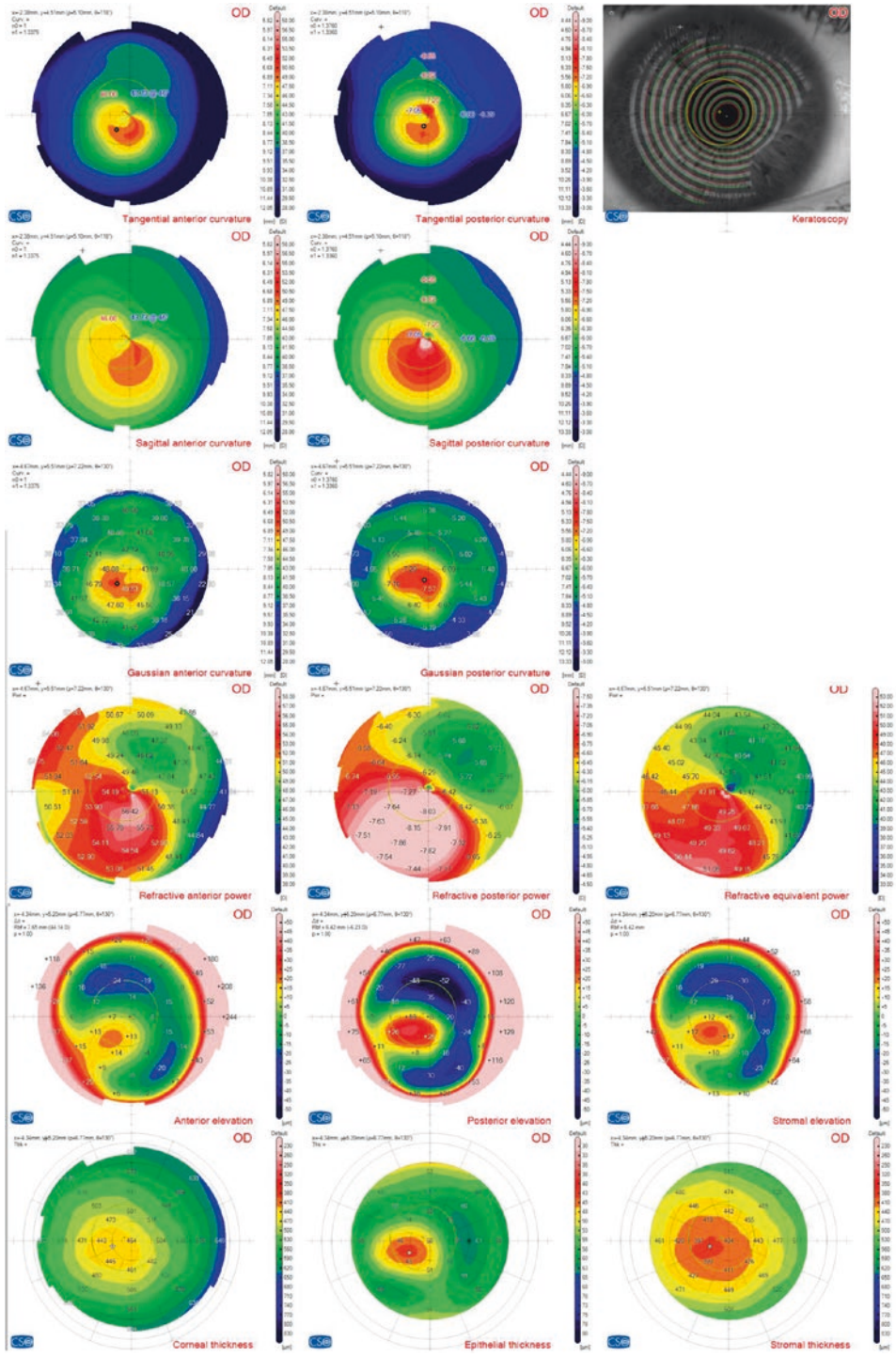

Fig. 29.9 Maps of a keratoconic eye. From top left corner: tangential anterior curvature, tangential posterior curvature, keratoscopy, sagittal anterior curvature, sagittal posterior curvature, Gaussian anterior curvature, Gaussian posterior curvature, refractive anterior power, refractive posterior power, refractive equivalent power, anterior elevation, posterior elevation, stromal elevation, corneal thickness, epithelial thickness, and stromal thickness

allows a more solid earlier diagnosis of keratoconus, as epithelial changes precede changes on the anterior corneal surface. An epithelial doughnut pattern, characterized by epithelial thinning surrounded by an annulus of thicker epithelium [7, 8], coincident with the bulging zone of the posterior elevation and the steepening of the posterior corneal surface, is consistent with keratoconus and it reinforces its diagnosis. Second, epithelial thickness profiles may be helpful in excluding a misdiagnosis of keratoconus when the topography of anterior corneal surface is suspect. An epithelial thickening over an area of topographic steepening implies that the steepening is due to the epithelium and not to an underlying ectatic surface. Asymmetrical topographic patterns and focal anterior steepening can sometimes be secondary to corneal warpage: analysis of the epithelial layer with high-resolution AS-OCT allows for direct detection of the abnormality rather than just supposing it.

In addition to keratoconus screening, corneal epithelial mapping provides a practical tool in a variety of other clinical applications. It allows for the measurement of corneal epithelial thickness changes following laser ablative myopic surgeries, such as LASIK [11–17], PRK [18–21], and small incision lenticule extraction (SMILE) [22]. Studies have suggested that epithelial thickening is associated with myopic regression after LASIK as well as PRK, although the wound healing process would be quite different in the two procedures [12, 18, 20]. It also allows for the quantitative analysis of the effects of an orthokeratology treatment [23–27] or the anatomical evaluation of corneal changes induced by intracorneal ring segments implantation [28].

IOL Module

CSO's method for IOL calculation is an attempt to apply the most advanced engineering method used for optical system design and analysis to IOL calculation. The method is intended to keep a good accuracy not only with normal eyes but also with eyes, which underwent refractive surgery or with a heavy amount of astigmatism or with even more irregular corneas (keratoconic eyes or post-graft eyes after DMEK or DSAEK). The measured data of the anterior segment, i.e., the altimetric data of the anterior and posterior corneal surfaces and of the iris are used in combination with the altimetric data of the intraocular lens to build a three-dimensional model of the eye. In this way, the corneal surfaces are considered with their possible asymmetry, inclination, mutual decentration, and irregularities. The intraocular lens is modeled using the nominal parameters provided by its manufacturer. Possible aspherical profiles can be taken into account as well as possible torical shapes.

Ray tracing is used in order to simulate the path of light inside the eye. The calculation is done by the software for each available power of the selected IOL model. For the lens, which best satisfy the requirement of target equivalent sphere chosen by the surgeon, the following results are shown:

- refraction (sphere, cylinder, axis, and spherical equivalent)
- wave front aberrations
- refractive map
- point spread function (PSF)
- defocus chart

These results can also be consulted by the user for those lenses whose powers are included in an interval centred around the power of the best lens. If the IOL model is toric, the software makes the results available for each of the available IOL cylinders. Further details about CSO's method for IOL calculation will be given in a dedicated chapter of this book.

Toric IOL Marker

CSO's software also offers the clinician a useful tool (Camellin's marker) for marking the axis of a toric IOL and some reference points on a frontal image of the eye, which can be printed and used as a reference for the IOL alignment during surgery (Fig. 29.10). The basic idea is to use a frontal colour image of the eye captured by the

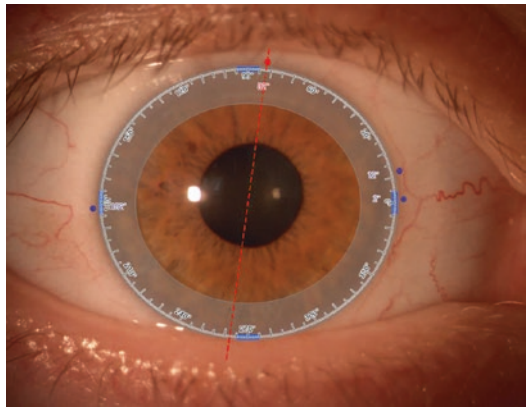

Fig. 29.10 Toric marker: the axis of the IOL is represented by the dotted red line; the violet circles are the reference points

slit lamp. For a correct use of the toric marker, it is necessary to use the 10x magnification lens in CSO slit lamp microscope. This is the only magnification, which allows the user to see the entire eye. The user has to translate and deform a goniometer so that it matches the limbus of the eye (Fig. 29.7). The goniometer will be used as a reference for the angular position of the IOL axis.

After that, the user has to place 3 small violet discs near some reference vessels on the sclera and rotate the axis of the IOL at the desired angle. Of course, it is also necessary to choose an image of the eye where the vessels are well visible on the sclera.

The toric marker is accessible from both the slit lamp environment and the IOL module. In the IOL module, the user can also associate an axial map to the picture of the toric marker.

References

1. Mejía-Barbosa Y, Malacara-Hernández D. A review of methods for measuring corneal topography. Optom Vis Sci. 2001;78(4):240–53.
2. Huang D, et al. Optical coherence tomography. Science. 1991;254(5035):1178–81.
3. Wojtkowski M, Leitgeb R, Kowalczyk A, Bajraszewski T, Fercher AF. In vivo human retinal imaging by Fourier domain optical coherence tomography. J Biomed Opt. 2002;7:457–63.
4. Vakhtin AB, Kane DJ, Wood WR, Peterson KA. Common-path interferometer for frequency-domain optical coherence tomography. Appl Opt. 2003;42:6953–8.
5. Scroggs MW, Proia AD. Histopathological variation in keratoconus. Cornea. 1992;11:553–9.
6. Aktekin M, Sargon MF, Cakar P, Celik HH, Firat E. Ultrastructure of the cornea epithelium in keratoconus. Okajimas Folia Anat Jpn. 1998;75:45–53.
7. Reinstein DZ, Archer TJ, Gobbe M. Corneal epithelial thickness profile in the diagnosis of keratoconus. J Refract Surg. 2009;25:604–10.
8. Reinstein DZ, Gobbe M, Archer TJ, Silverman RH, Coleman DJ. Epithelial, stromal, and total corneal thickness in keratoconus: three-dimensional display with Artemis very high-frequency digital ultrasound. J Refract Surg. 2010;26:259–71.
9. Temstet C, Sandali O, Bouheraoua N, Hamiche T, Galan A, El Sanharawi M, Basli E, Laroche L, Borderie V. Corneal epithelial thickness mapping using Fourier-domain optical coherence tomography for detection of form fruste keratoconus. J Cataract Refract Surg. 2015;41(4):812–20.
10. Li Y, et al. Corneal epithelial thickness mapping by Fourier-domain optical coherence tomography in normal and Keratoconic eyes. Ophthalmology. 2012;119(12):2425–33.
11. Kanellopoulos AJ, Asimellis G. Longitudinal postoperative Lasik epithelial thickness profile changes in correlation with degree of myopia correction. JRefract Surg. 2014;30:166–71.
12. Lohmann CP, Güell JL. Regression after LASIK for the treatment of myopia: the role of the corneal epithelium. Semin Ophthalmol. 1998;13:79–82.
13. Reinstein DZ, Silverman RH, Sutton HF, Coleman DJ. Very high-frequency ultrasound corneal analysis identifies anatomic correlates of optical complications of lamellar refractive surgery: anatomic diagnosis in lamellar surgery. Ophthalmology. 1999;106:474–82.
14. Spadea L, Fasciani R, Necozione S, Balestrazzi E. Role of the corneal epithelium in refractive changes following laser in situ keratomileusis for high myopia. J Refract Surg. 2000;16:133–9.
15. Erie JC, Patel SV, McLaren JW, Ramirez M, Hodge DO, Maguire LJ, Bourne WM. Effect of myopic laser in situ keratomileusis on epithelial and stromal thickness: a confocal microscopy study. Ophthalmology. 2002;109:1447–52.
16. Patel SV, Erie JC, McLaren JW, Bourne WM. Confocal microscopy changes in epithelial and stromal thickness up to 7 years after LASIK and photorefractive keratectomy for myopia. J Refract Surg. 2007;23:385–92.
17. Reinstein DZ, Srivannaboon S, Gobbe M, Archer TJ, Silverman RH, Sutton H, Coleman DJ. Epithelial thickness profile changes induced by myopic LASIK as measured by Artemis very high-frequency digital ultrasound. J Refract Surg. 2009;25:444–50.
18. Lohmann CP, Patmore A, Reischl U, Marshall J. The importance of the corneal epithelium in excimer-laser photorefractive keratectomy. Ger J Ophthalmol. 1996;5:368–72.

19. Gauthier CA, Holden BA, Epstein D, Tengroth B, Fagerholm P, Hamberg-Nyström H. Role of epithelial hyperplasia in regression following photorefractive keratectomy. Br J Ophthalmol. 1996;80:545–8.
20. Lohmann CP, Reischl U, Marshall J. Regression and epithelial hyperplasia after myopic photorefractive keratectomy in a human cornea. J Cataract Refract Surg. 1999;25:712–5.
21. Chen X, Stojanovic A, Liu Y, Chen Y, Zhou Y, Utheim TP. Postoperative changes in corneal epithelial and stromal thickness profiles after photorefractive keratectomy in treatment of myopia. J Refract Surg. 2015;31:446–53.
22. Luft N, Ring MH, Dirisamer M, Mursch-Edlmayr AS, Kreutzer TC, Pretzl J, et al. Corneal epithelial remodeling induced by small incision Lenticule extraction (SMILE). Invest Ophthalmol Vis Sci. 2016;57:176–83.
23. Reinstein DZ, Gobbe M, Archer TJ, Couch D, Bloom B. Epithelial, stromal and corneal pachymetry changes during orthokeratology. Optom Vis Sci. 2009;86:E1006–14.
24. Swarbrick HA, Wong G, O'Leary DJ. Corneal response to orthokeratology. Optom Vis Sci. 1998;75:791–9.
25. Lu F, Simpson T, Sorbara L, Fonn D. Malleability of the ocular surface in response to mechanical stress induced by orthokeratology contact lenses. Cornea. 2008;27:133–41.
26. Sridharan R, Swarbrick H. Corneal response to short-term orthokeratology lens wear. Optom Vis Sci. 2003;80:200–6.
27. Haque S, Fonn D, Simpson T, Jones L. Epithelial thickness changes from the induction of myopia with CRTH RGP contact lenses. Invest Ophthalmol Vis Sci. 2008;49:3345–50.
28. Reinstein DZ, Srivannaboon S, Holland SP. Epithelial and stromal changes induced by intacs examined by three-dimensional very high-frequency digital ultrasound. J Refract Surg. 2001;17:310–8.